Remote Sensing of Environment 237 (2020) 111525

Contents lists available at ScienceDirect

Remote Sensing of Environment

journal homepage: www.elsevier.com/locate/rse

Quantifying fire trends in boreal forests with Landsat time series and self-organized criticality

Akira Kato[a,*], David Thau[b], Andrew T. Hudak[c], Garrett W. Meigs[d], L. Monika Moskal[e]

[a] Graduate School of Horticulture, Chiba University, 648 Matsudo Matsudo, Chiba, 2710092, Japan
[b] World Wildlife Fund, 1250 24th Street, N.W. Washington, DC, 20037, USA
[c] Rocky Mountain Research Station, USDA Forest Service, Forestry Sciences Laboratory, 1221 South Main Street, Moscow, ID, 83843, USA
[d] College of Forestry, Oregon State University, 321 Richardson Hall, Corvallis, OR, 97333, USA
[e] School of Environmental and Forest Sciences, University of Washington, Box 352100 Seattle, WA, 98195, USA

ARTICLE INFO

Keywords:
Forest fire
Self-organized criticality
Google earth engine
Boreal forest
Landsat
Time-series analysis
Image compositing
Fractal
NDVI
NBR
Fire perimeter
Fire refugia
Mosaic landscape

ABSTRACT

Boreal forests are globally extensive and store large amounts of carbon, but recent climate change has led to drier conditions and increasing fire activity. The objective of this study is to quantify trends in fire size and frequency using data spanning multiple scales in space and time. We use multi-temporal Landsat image compositing on Google Earth Engine and validate results with reference fire maps from the Canadian Park Service. We also interpret general fire trends through the concept of Self-Organized Criticality (SOC). Our study site is Wood Buffalo National Park, which is a fire hot spot in Canada due to frequent lightning ignitions. The relativize differenced normalized burn ratio (RdNBR) was the most accurate Landsat-based burn severity metric we evaluated (52.2% producer's accuracy, 87.6% user's accuracy). The Landsat-based burn severity maps provided a better fit for a linear relationship on the log-log scale of fire size and frequency than a manually drawn fire map. Landsat-based fire trends since 1990 conformed to a power-law distribution with a slope of 1.9, which is related to fractal dimensions of the satellite-based fire perimeter shapes. The unburned and low-severity patches within the burn severity mosaic influenced the power-law slope and associated fractal dimensionality. This study demonstrates a multi-scale and multi-dataset technique to quantify general fire trends and changing fire cycles in remote locations and establishes a baseline database for assessing future fire activity. Testing criticality by power laws helps to quantify emergent trends of contemporary fire regimes, which could inform the strategic application of prescribed fire and other management activities. Natural resource managers can utilize information from this study to understand local ecosystem adaptability to large fire events and ecosystem stability in the context of recent increasing fire activity.

1. Introduction

Over thirty percent of terrestrial global carbon is stored in boreal forests, which represents a major sink absorbing CO_2 from the Earth's atmosphere (Kasischke et al., 1995). Recent climate change indirectly causes increasing forest fire activity, especially in the boreal forest region via large-scale atmospheric circulation change (Amiro, 2001; Kasischke and Turetsky, 2006; Skinner et al., 2002). The broad circumboreal forest, including Canada, Russia, and Alaska (Flannigan et al., 2015), is vulnerable to drier climate conditions caused by temperature rise (Kasischke and Turetsky, 2006). To monitor and track large-scale changes, remote sensing techniques are an essential means to identify tipping points and detect altered ecosystems (Barnosky et al., 2012). Remote sensing techniques are additionally important for forest fire monitoring in the boreal forest region due to difficult accessibility, and the spatial scale of the boreal forest requires economically feasible ways to use publicly available images like Landsat imagery from the United States Geological Survey (USGS) and Sentinel images from the European Space Agency.

To help diverse users access and analyze geospatial data, Google Earth Engine (GEE) provides a cloud-based platform and a user-friendly interface to display and analyze freely provided petabytes of satellite-based and other imagery using built-in functions orchestrated by JavaScript and Python programming interfaces. GEE promotes the accessibility of the publicly available data for any level of scientists, general public, and policy makers who need to analyze geospatial information without the burden of downloading large amounts of data (Gorelick et al., 2017), which enables novel applications and

* Corresponding author.
E-mail address: akiran@faculty.chiba-u.jp (A. Kato).

https://doi.org/10.1016/j.rse.2019.111525
Received 4 April 2019; Received in revised form 3 November 2019; Accepted 4 November 2019
Available online 15 November 2019
0034-4257/

assessments of boreal fire activity. GEE has been used for analyzing various scales from global (Hansen et al., 2013) to local (Soulard et al., 2016) vegetation change mapping and monitoring.

In general, forest fire regimes are described by fire frequency, intensity, and extent (Agee, 1993; Sugihara et al., 2006). All three attributes are related to fire behavior, which is defined by three-way interactions among topography, fuel, and fire weather (Sugihara et al., 2006). It is important to understand contemporary fire extent and frequency in terms of the historical range of variability, but the application of the historical range to forest management is complicated by recent climate change (Keane et al., 2009). For example, shorter cycles of stand-replacing fire reduce stand density and residual tree height, which influences the landscape mosaic and impacts fire refugia, post-fire species composition, and trajectories of fuel accumulation (Meddens et al., 2018; Schoennagel et al., 2017; Turner et al., 2001). Changing fire regimes also makes it more difficult to understand general fire trends in the contemporary fire record (Reilly et al., 2017).

To measure general forest fire trends, a heuristic approach called Self-Organized Criticality (SOC) has been proposed (Bak, 1996) and utilized to understand trends of sporadically occurring natural hazards (Malamud and Turcotte, 1999). The theory was initially demonstrated from a sandpile model (Bak, 1996) and has been applied to natural disasters such as earthquakes and forest fires (Albano, 1995; Drossel and Schwabl, 1992; Hergarten, 2002; Malamud et al., 1998; Malamud and Turcotte, 1999; Perry, 1995; Ricotta et al., 2001, 1999; Siegfried et al., 1996; Song et al., 2001). If the forest condition reaches a critical state (self-cycle state), any change caused by natural events follows the power-law distribution between their size and frequency and forms a straight line on log-scaled x and y axes (Fig. 1). If the size and frequency are separately displayed, the data match between them is not clear (left side of Fig. 1). However, if they are plotted in the log-log scales (the right side of Fig. 1), the slope indicates trends of the disturbance events. A steeper slope represents smaller sized events occurring on a more frequent basis (Malamud and Turcotte, 1999). To obtain the slope, continuous and long-term observation data are required (Ricotta et al., 2001, 1999; Song et al., 2001).

Collecting long-term fire records is labor intensive and limited by the spatial interpolation of discrete samples. For example, charcoal records in lake sediment and tree-ring records are from discrete sample locations and are not necessarily applicable to contemporary fire regimes (Bowman et al., 2011; MacDonald et al., 1991). To understand a large-scale fire trends, a fire scar network was established to collect more widespread samples across large areas (Falk et al., 2011). However, time series data can be derived from the digital image archives of satellite imagery available from long-term Landsat observations since the 1970s. Multi-temporal Landsat image analysis makes it feasible to track contemporary fire frequency and the area burned in a spatially explicit manner (Meddens et al., 2018). To map forest fires, the pre- and post-fire difference of the Normalized Burn Ratio (NBR) has been extensively used for applications such as Burned Area Reflectance Classification (BARC, Geospatial Technology and Application Center, USDA Forest Service), Monitoring Trends in Burn Severity (MTBS), and Rapid Assessment of Vegetation Condition after Wildfire (RAVG, USDA Forest Service). However, until recently general forest fire trends (including whether large or small fire activity is increasing) have not been quantified automatically from satellite observations due to landscape complexity and data limitations.

In addition to satellite imagery, fire maps are also created by local agencies. Although such locally derived fire maps represent the best available ground truth for long-term records, there are some specific challenges for accuracy assessments. Specifically, the data were commonly prepared by drawing fire perimeter outlines, which can include errors and generalized fire patterns. Chuvieco and co-authors (2019) extensively reviewed burned area (BA) detection papers from all remotely sensed data and concluded that the standardized collection of remote sensing data can enable consistent data quality over space and time and overcome uncertainty of data analysis across different agencies and countries. The accuracy and precision of BA product are critical for identifying key fire-related environmental variables such as topography (Barros et al., 2013, 2012; Krawchuk et al., 2016), physiography and climate (Mansuy et al., 2014), and ecozone (Parisien et al., 2006) and creating scenarios of future global fire activity (Krawchuk et al., 2009). The spectral indices are effective ways to select images needed for BA detection from Landsat time-series in prior studies (Bastarrika et al., 2011; Goodwin and Collett, 2014; Hawbaker et al., 2017). A particularly important issue is the uncertainty of how fire perimeter

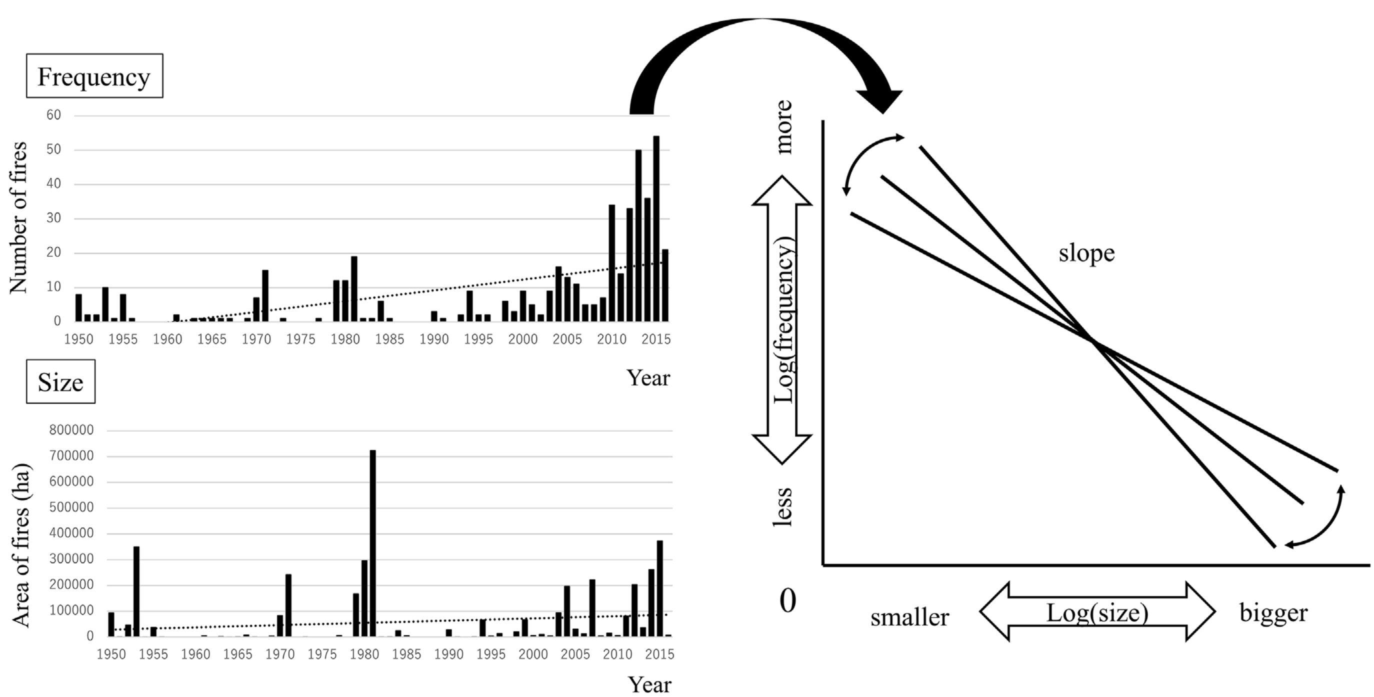

Fig. 1. The concept of Self-Organized Criticality.

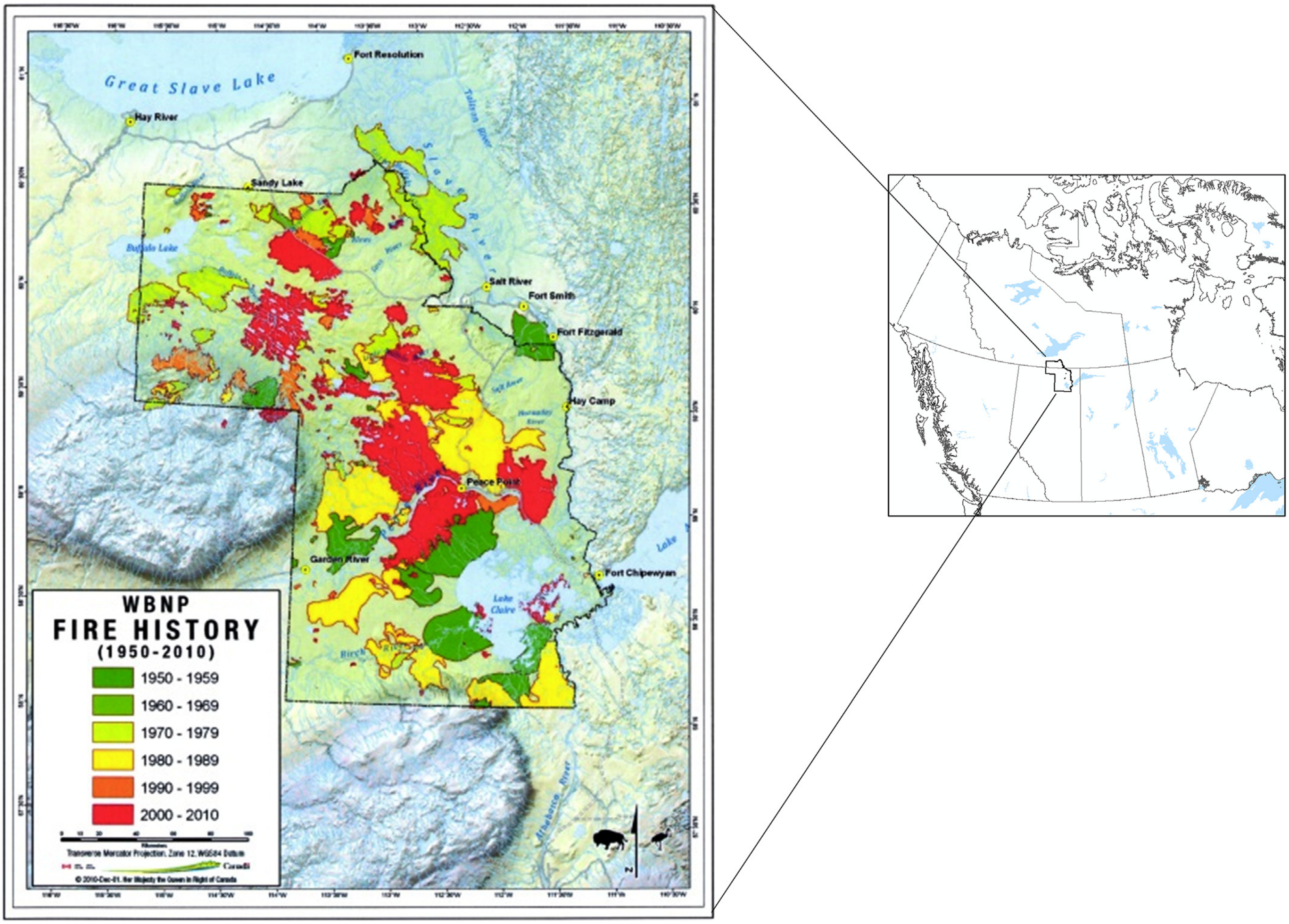

Fig. 2. Study site is located at Wood Buffalo National Park in the Northwest Territories, Canada (fire map is produced by Canadian Park Services).

polygons include unburned and low-severity areas (i.e., fire refugia; A.J.H. Meddens et al., 2018a).

The objectives of this study are: (1) to map fire extent and frequency usingmulti-temporal Landsat images and to validate these maps with existing manually drawn fire maps from the Canadian Park Service; (2) to compute and interpret general fire trends with the concept of Self-Organized Criticality. For the first objective, we use Google Earth Engine (GEE) to compute and evaluate the accuracy of dNBR and RdNBR (defined below) with maximum NDVI (pre-fire condition) and minimum NBR (post-fire condition) image composites during the fire season. For the second objective, we test the power-law distribution on log-log scales using Kolmogorov-Smirnov (KS) statistics and compare fire trends obtained from multi-temporal satellite data since 1990 with the reference map since 1950.

2. Study site

Our study site is Wood Buffalo National Park (WBNP) in the Northwest Territories and Alberta, Canada (Fig. 2). The park provided habitat for wildlife animals such as wood buffalo (*Bison bison athabascae*) and whooping crane (*Grus americana*). Trees composition is dominated mainly by jack pine (*Pinus banksiana*), aspen (*Populus tremuloides*), balsam poplar (*Populus balsamifera*), white spruce (*Picea glauca*), black spruce (*Picea. Mariana*), and tamarack (*Larix laricana*). In the site, fires are typically ignited by lightning (Campos-Ruiz et al., 2018; Kochtubajda et al., 2006) and need to be monitored. WBNP is one of the largest parks in North America and has had major fire events recorded since 1950s. The park is located in a fire hot spot of Canada (Gillett et al., 2004; Stocks et al., 2002). The number of fire events in recent years has gradually increased, and the total area burned has dramatically increased (Stocks et al., 2002). The forest fire cycle is around 70 years (Larsen et al., 2012), however the cycle varies among forest types from 39 to 96 years (Larsen, 1997). Our study site has no forest management activities and has been protected as national park since 1922, which makes it an ideal place to test SOC. To study general fire trends under the concept of self-organized criticality, we compare the fire cycle derived from long-term satellite images with that from a reference fire map. The park has been assessed with satellite-based fire monitoring in several prior studies (Larsen, 1997; Soverel et al., 2011, 2010; Wilson et al., 2018), however the fire maps created from prior efforts are different from the fire map created from this study using Landsat time-series analysis.

3. Methods

We use Landsat image archive on Google Earth Engine to create a new fire map using a composite image approach on time-series images (Chuvieco et al., 2008). To make clear images, a composite image approach has been applied using high frequency 1 km resolution global images for the Canadian boreal forest (Chuvieco et al., 2008). Prior BA mapping was restricted by the image resolution, although 1 km resolution was enough to detect fire ignition with only 1.8% false detection (Hantson et al., 2013). The two-phase approach (Bastarrika et al., 2011) has also been implemented successfully to detect BA. The accuracy of this method relies on the image quality of identified post-fire images during the first-phase, and multiple spectral indices can be

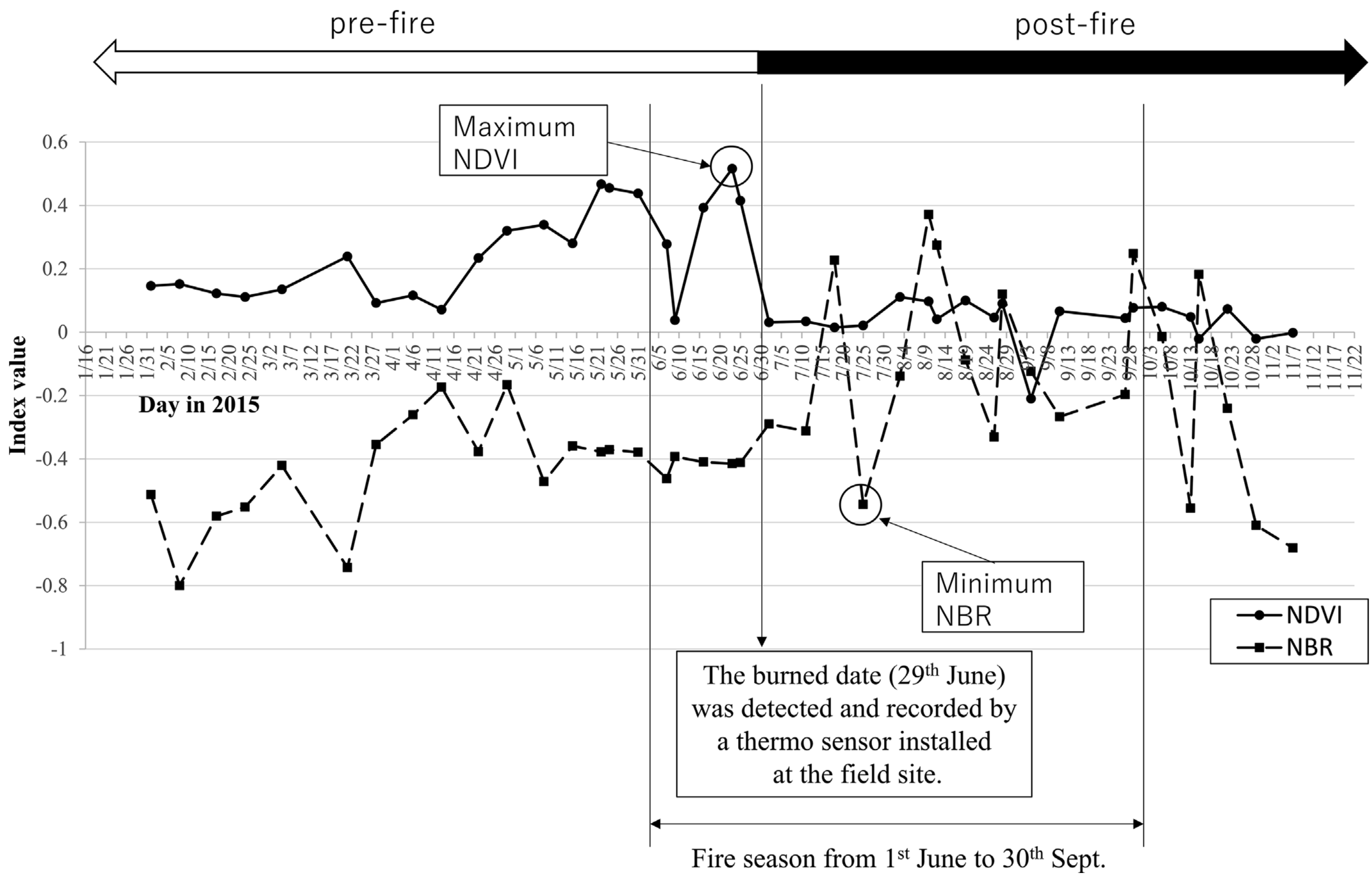

Fig. 3. The NDVI and NBR value change before and after fire during 2015. The maximum NDVI value was used to find pre-fire and the minimum NBR was used to find post-fire days within the fire season from 1st June to 30th Sept in this study site. This figure demonstrates that the maximum NDVI and minimum NBR can pick up pre- and post-fire days.

combined to reduce errors selected post-fire images. A particularly important advantage of the time-series approaches is the ability to conduct image compositing, which has been mainly applied to cloud-reduced mosaics created via multi-day image composites (Chuvieco et al., 2008; Parks et al., 2018) and maximum albedo-based image compositing (Barbosa et al., 1998). Image compositing can detect forest fire without any prior knowledge about when a fire occurred. When identifying forest fires, conventional satellite image analysis requires specific dates to select bi-temporal images (pre- and post-fire images) to assess fire severity (Epting et al., 2005; Roy et al., 2006), ideally by anniversary date to account for consistent phenological status (French et al., 2008; Lentile et al., 2009; Lu et al., 2004; Veraverbeke et al., 2010a). Choosing the scenes using a scene-based search adds unexpected spectral variation, contains different day time illumination in terrain conditions (Verbyla et al., 2008), and requires cloud free images. Although these difficulties can be addressed with calibration methods like the optimality method (Roy et al., 2006; Verstraete and Pinty, 1996) which enables less noisy spectral reflectance using the distance and angle change in the two spectral domains, compositing is a more powerful way to leverage the full information content of available data. In this study, to avoid the challenges of the scene-based approaches, we apply a pixel-based image compositing approach (White et al., 2014) to track fire-induced change at the pixel scale. Satellite images used for image compositing in this study were from the top of atmosphere (TOA) Tier 1 Landsat image collection and we included only images with less than 10% cloud cover according to the collection metadata. We computed key spectral indices, including NBR and NDVI. NBR is the differentiated value between short-wave infrared and near infrared red spectral band, while NDVI is the differentiated value between near-infrared red and red spectral band.

$$NBR = 1000 \times (\rho MIR - \rho NIR)/(\rho MIR + \rho NIR)$$

$$NDVI = (\rho NIR - \rho Red)/(\rho NIR + \rho Red)$$

The areas burned by fire are identified by the indices below (Miller and Thode, 2007).

$$dNBR = (NBR_{prefire} - NBR_{postfire})$$

$$RdNBR = dNBR / \sqrt{ABS(NBR_{prefire}/1000)}$$

where ρ MIR is Mid-Infrared, ρ NIR is Near-Infrared, and ρ Red is red spectral reflectance band. The NBR and RdNBR ranges from −1000 to 1,000, and dNBR ranges from −2000 to 2000 (Key and Benson, 2006).

The reference fire map was provided by the Canadian Park Service from 1950 to 2016 as fire boundary polygons, which were digitized manually and updated within the park from several resources such as satellite images, historical aerial photos, and GPS collection from field crews.

Conventionally, the specific date of fire is identified using the spectral change over a given Landsat scene or region (Cohen et al., 2010; Kennedy et al., 2010; Zhu and Woodcock, 2014). However, this study uses composite images based on specific indices. For example, a maximum NDVI composite image is a single image derived from a time-series of images. Each pixel in the maximum NDVI composite stores the spectral values from the pixel in the time-series stack at that location with the maximum NDVI value. This image composite process mitigates cloud and shadow effects, because the indices go to zero when the pixel has the same values of all bands over cloud and shadow. Even though WBNP has flat terrain and has minimal topographic effects, the lower azimuth sun angle in the high latitude causes lower illumination and reflectance values. In this case, the image compositing process maximizes the opportunity to collect more illuminated pixels to mitigate this effect. GEE has a collection of image processing algorithms to identify the area burned from multi-temporal images. There is also a series of image compositing functions to compute a value by pixel from a stack of multi-temporal images. Pixel-based analysis through GEE is faster than conventional for-loop commands with a kernel visiting each pixel, because in GEE all pixel values are computed in parallel across multiple computers (Gorelick et al., 2017).

We only analyzed satellite images during the fire season, which runs from June 1st to September 30th. The spectral reflectance of the maximum NDVI during the season is assumed to represent pre-fire conditions, and the spectral reflectance of the minimum Normalized Burn Ratio (NBR) during the season is assumed to represent post-fire conditions (Fig. 3). Fig. 3 demonstrates how the spectral indices enable identification of pre- and post-fire days within the fire season. The maximum NDVI and minimum NBR are only searched within the fire season because mid-Infrared spectral region is sensitive to snow. Outside of the range, NBR values goes under the minimum and is not related to fire. For the site used to create Fig. 3, the fire came to the site where a thermal sensor was installed. The sensor detected and recorded the actual day of burn. For each pixel, the pre- and post-fire date are identified to store values to make an image composite for all bands, then NBR is computed from the pre-fire and post-fire composite images. The difference between the two NBR images is then used to compute dNBR and RdNBR. The year range of satellite images used in this study is from 1986 to 2016, which includes the Landsat 5, 7, and 8 sensors. We used the best combination of different sensors, and the sensor availability is the overlap of sensor duration: Landsat 5 is used from 1990 to 2011, Landsat 7 is used from 1999 to 2016, and Landsat 8 is used from 2014 to 2016.

When identifying burned area using dNBR or RdNBR, we implemented a threshold to avoid subjective decisions using the Otsu method (Otsu, 1979). The Otsu method has been used to determine the threshold in a bimodal distribution to create a binary image in computer vision (Shapiro and Stockman, 2001). When the bimodal distribution is divided into two regions, the Otsu method finds the threshold point that minimizes the inter-class variance (Otsu, 1979). The implementation of the Otsu method requires both burned and unburned areas. The unburned area is collected using the minimum bounding boxes from the surrounding area burned. Because the spectral calibration is variable among Landsat sensors, we computed the threshold value computed by each sensor (Landsat 5, 7 and 8) for dNBR and RdNBR respectively. After computing threshold values for dNBR and RdNBR, we chose one fixed threshold value to apply to all data to maintain a consistent thresholding process.

After creating the binary images (value 1 is assigned for the area burned and value 0 is for unburned) from dNBR or RdNBR images, there was still noise left in the images so we applied multiple noise filtering steps (see Fig. 4). The first filtering removed water bodies (lake or stream) using NDVI more than 0.2 in a maximum NDVI composite image. The second filtering removed small segments using connected component analysis, which labels separate index numbers to all segments and computes the area for each. The segments with an area less than 3 ha are removed through this step. The 3 ha is similar to the striping noise on images (mainly on Landsat 7 images). After the first and second filtering steps were applied, we smoothed the remaining area using morphological image operations (Shapiro and Stockman, 2001). The smoothing process is required to make the result comparable to the reference data which has a smoothly outlined fire perimeter (Goodwin and Collett, 2014; Zhang, 2008). Morphological image filtering with opening and closing operations is applied with a 5 x 5 window to remove isolated noise on the binary image. To complete the process, we saved the burned area results as a mask. We retained the burned area mask in the following 10 years to avoid duplicated areas burned in the following years.

We evaluated the satellite results using a reference map provided by the Canadian Park Service, which we used for accuracy assessment (user's and producer's accuracy and commission and omission errors). There are important challenges when comparing results between satellite-based analysis and manually digitized reference data. The reference polygon is drawn as an outline representing a fire perimeter and does not capture the detailed mosaic patterns inside the boundary, including variations in burn severity and unburned areas. Relatively low accuracy values stem from this unavoidable technical difference. To understand this effect, we prepared and created fire perimeter boundaries excluding any interior unburned patches from satellite results to conduct the accuracy assessment.

3.1. The concept of self-organized criticality

To understand the relationship between the area burned and the frequency of forest fire, the two are plotted in log-log XY space to assess whether they follow the power-law distribution, which indicates a critical (self-maintained) state (Malamud and Turcotte, 1999). When the power-law relationship is indicated, the slope of the size-frequency relationship provides the general trends of forest fire. To validate the log-log scale and relationship, we applied a validation technique proposed by Clauset et al. (2009). The power-law distribution is formulated below.

$$p(\mathrm{x}) \sim \mathrm{x}^{-\alpha.}$$

This implies the log-log scale formula below.

$$\log p(\mathrm{x}) = -\alpha \log(\mathrm{x}) + \mathrm{c}$$

Where the probability density of $p(x)$ is the frequency or histogram of x, α is the scaling factor of this power-law, and c is the noise and constant which is not normally distributed because of the transposed logarithm value.

To test whether the distribution follows the power-law or not, Clauset et al. (2009) provide two steps. First, maximum likelihood estimators are used in the doubly logarithmic axes to determine the scaling parameter α (the slope) of the equation above. Second, the lower bound x_{min} is determined. The power-law relationship is only established when x is above some lower bound x_{min}. We used, the Kolmogorov-Smirnov (KS) statistic to quantify x_{min} and to identify the best fit of the power-law distribution with the condition: $x > x_{min}$. The KS statistic is

$$D = \max_{x \geq xmin} |P_{emp}(x) - P_{power}(x)|$$

where $P_{emp}(x)$ is the empirical cumulative distribution function (CDF) and $P_{power}(x)$ is the CDF of the power-law model best fitted to $P_{emp}(x)$. The minimum value of D can be chosen with variable values of x_{min}.

With the determined variables of α and x_{min}, we conducted *a goodness-of-fit test* for the relationship between the fire extent and frequency. The hypothesis (the two distributions are the same) is tested using the distance between the empirical and the power-law through bootstrap sampling. If the *p*-value is more than 0.05, the difference is within the variation expected statistically. If it is less than 0.05, the power-law is ruled out. When the relationship follows a power-law distribution, the system reaches the self-organized state.

4. Results

(1) Fire mapping with Landsat multi-temporal image analysis using GEE

Based on the Otsu method (Fig. 5), the threshold values for each Landsat sensor between burned and unburned values was 584.31 for both the dNBR and RdNBR indices. The main difference between the two indices is the smaller burned extent detected by dNBR compared to

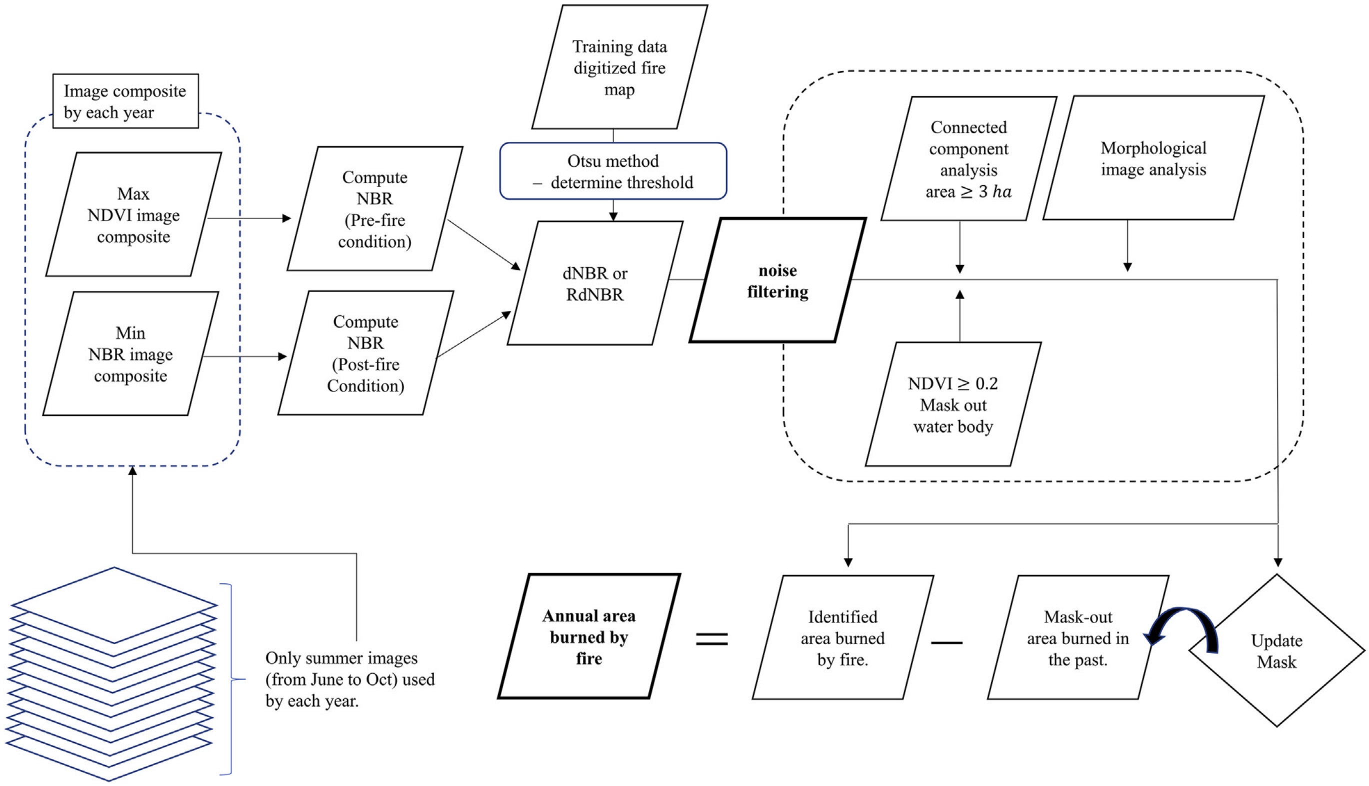

Fig. 4. Schematic diagram on Google Earth Engine analysis.

RdNBR, which occurred because the normalization of RdNBR with pre-fire vegetation expanded the area (A and D in Fig. 6). RdNBR was better in identifying the area burned than dNBR when compared with the reference data, but dNBR better avoided misclassifying unknown pixels than RdNBR (Fig. 7). Fig. 7 showed that RdNBR detects more area than dNBR because of the normalization of RdNBR. In addition, when creating fire boundaries, RdNBR matched the reference map better than dNBR did. When noise filtering was applied, the user's accuracy increased from 87.3% to 93.3% and 63.1% to 87.6% for dNBR and RdNBR respectively (Table 1). The overall producer's accuracy of RdNBR was better than that of dNBR by 13.6% while user's accuracy exhibited only a 5.7% difference between two (Table 1). As a result, RdNBR (with noise filtering) was optimal for creating annual fire maps from multi-temporal Landsat images.

After RdNBR was found to be optimal, an accuracy assessment was conducted only for RdNBR with the referenced fire map to provide

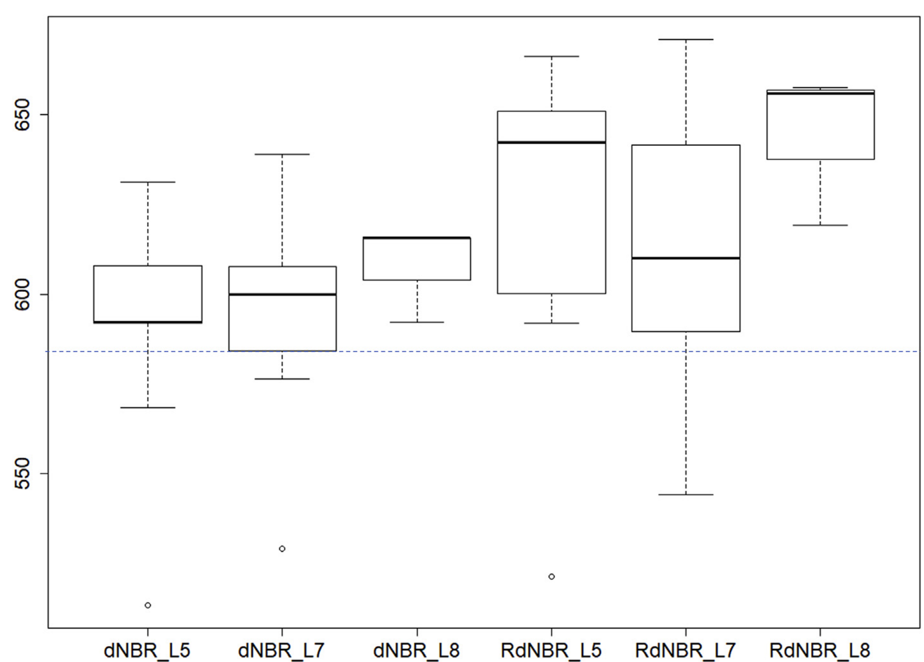

Fig. 5. The collection of threshold values of various Landsat sensors for dNBR and RdNBR from bounding box analysis. The dashed line is one threshold value set and used for this study.

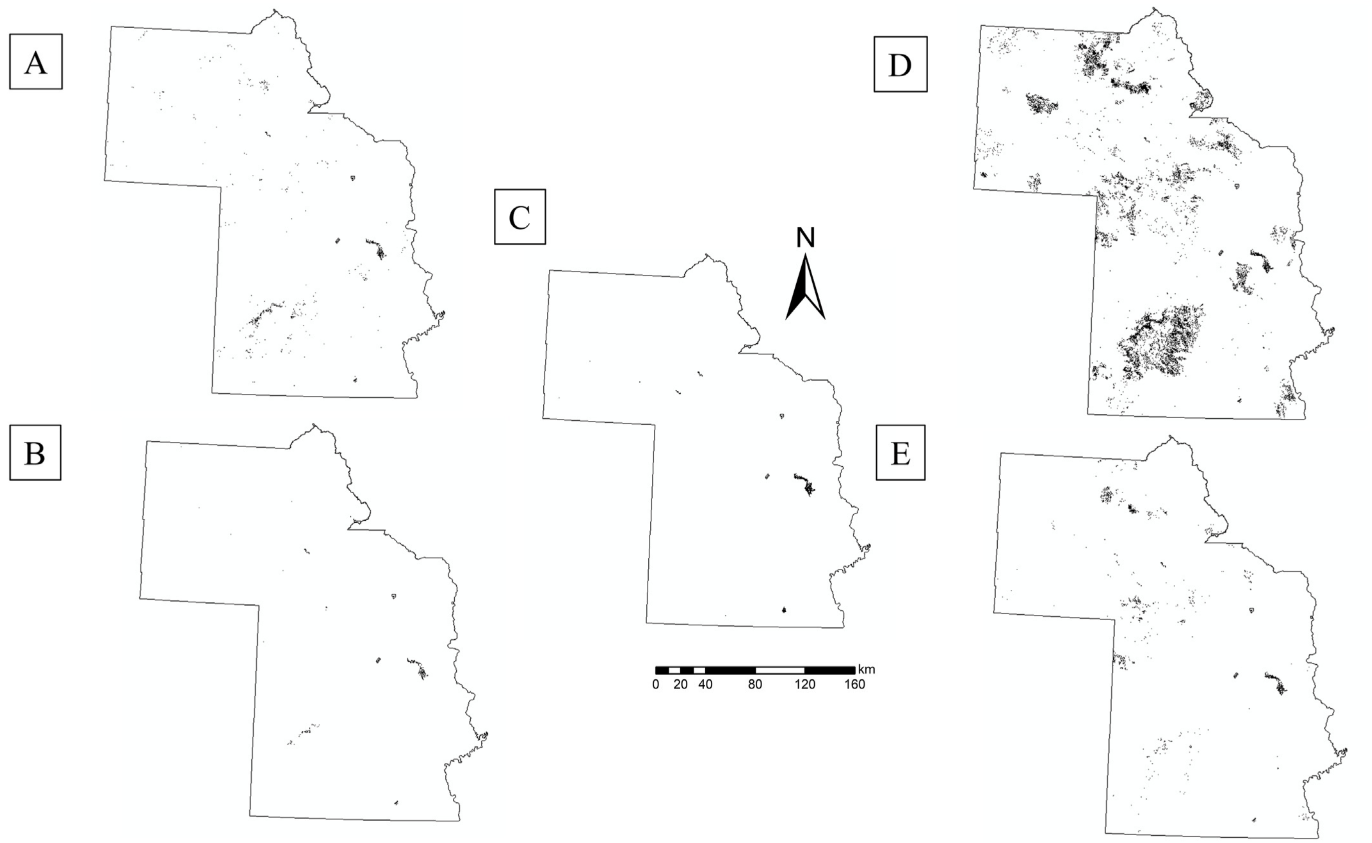

Fig. 6. dNBR and RdNBR images with and without filtering noises (2016 forest fire case, A: dNBR without noise removal, B: dNBR with noise removal, C: reference 2016 fire map from Canadian Park Services, D: RdNBR without noise removal, E: RdNBR with noise removal).

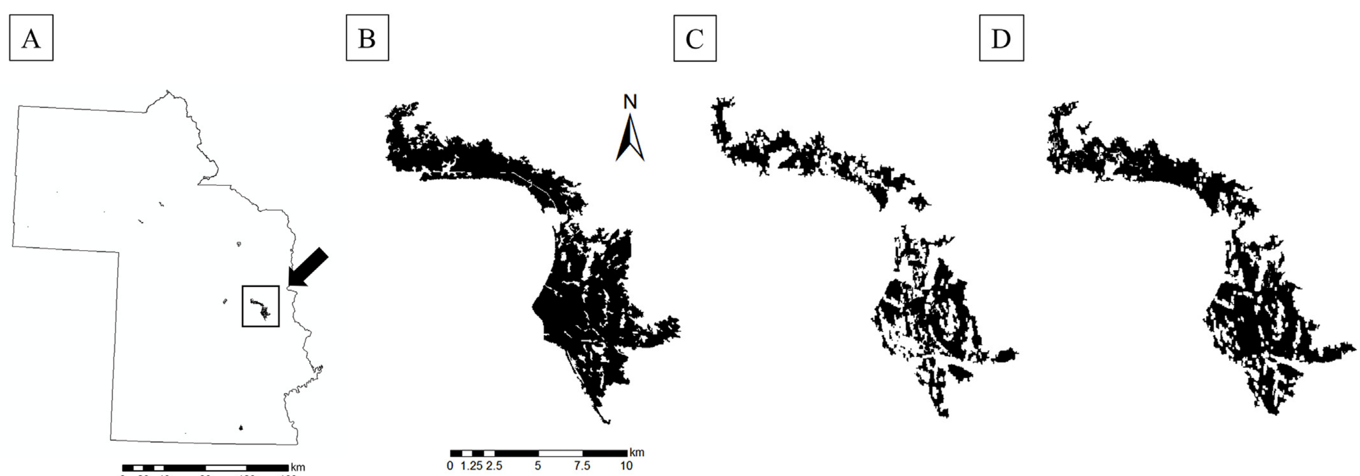

Fig. 7. dNBR and RdNBR images with filtering noise (A: the location from 2016 data in our research site, B: reference data, C: dNBR result, D: RdNBR result).

Table 1
Overall accuracy assessment before and after the noise filtering for dNBR and RdNBR.

(unit: %)	index	user's accuracy	producer's accuracy	commission errors	omission errors
Before noise filtering	dNBR	87.3	41.0	59.0	12.7
	RdNBR	63.1	55.9	44.1	36.9
After noise filtering	dNBR	93.3	38.6	61.4	6.7
	RdNBR	87.6	52.2	47.8	12.4

overall producer's and user's accuracy by each year (Fig. 8). From Fig. 8, the accuracy depended on the size of BA; small areas had wide variation of accuracy, while large areas had relatively higher accuracy. The weighted average of producer's accuracy was 52.2% and user's accuracy was 87.6%.

To show the effect of noise filtering, we presented the increasing and decreasing errors as a percentage (100% is the initial area of the misclassified error) and sorted by the area before the noise filtering. More than 100% means increasing misclassification after the noise filtering (left in Fig. 9), and less than 100% means decreasing misclassification after the noise filtering (right in Fig. 9). The commission errors were increased by 9.1% (the weighted average) and omission

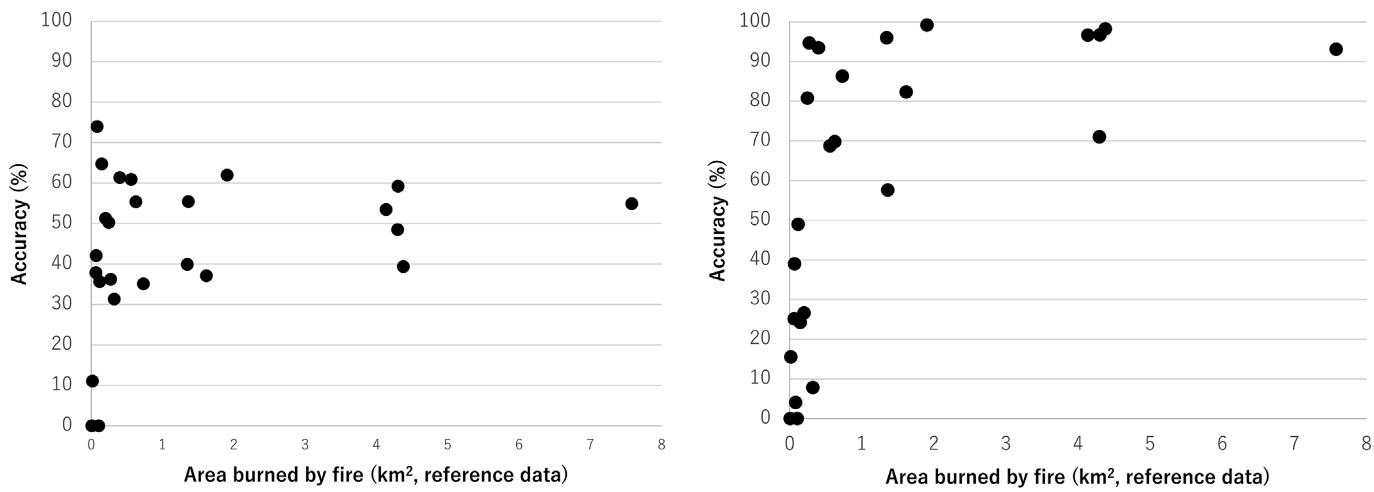

Fig. 8. RdNBR user's and producer's accuracy of this analysis (left: producer's accuracy, right: user's accuracy).

errors decreased dramatically by 82.9% (the weighted average) when 100% was set to the area of errors before the noise filtering was applied. Thus, the noise filtering used in this study significantly reduced the omission errors without substantially increasing commission errors.

Fig. 10 shows the difference between satellite results including unburned patches and manually digitized reference data excluding unburned patches. After unburned patches are excluded from satellite results to compare the accuracy with the reference data, the accuracy was increased from 52.2% to 62.0% (increased by 10%) for the producer's accuracy while 87.6% of user accuracy was the same.

(2) General trends of fire with the concept of self-organized criticality

The general fire trends obtained in the log-log space indicated a linear distribution from satellite results and a curved (non-linear) distribution from the reference map (Fig. 11). The slopes were 1.91 for the satellite imagery and 1.73 for the reference data (Table 2). The slope from the satellite result was steeper than that of the reference map. The minimum area that did not include the power-law relationship was 0.49 km^2 for the satellite map and 29.46 km^2 for the reference map, respectively. The bootstrap hypothesis testing using KS statistics rejected the distribution of the reference map (p value < 0.05), indicating that the distribution was not power-law. However, the satellite result was not rejected (p value > 0.05), indicating a power-law distribution. The goodness-of-fit based on KS statistics also indicated that the satellite result was closer to a power-law distribution than the reference map was. Fig. 12 shows the sensitivity of slopes by the different observation intervals from 1990 to 2000 (10 years), from 1990 to 2005 (15 years), from 1990 to 2010 (20 years), and from 1990 to 2016 (26 years). The longest interval was derived by the referenced data from 1950 to 2016 (66 years). The slopes from the reference map and the satellite result exhibited different sensitivities and responded differently to recent large fire events. The slope from the reference data since 1990 changed from 1.5 to 1.7 with the last six years especially influenced by large fire events, while the slope of reference data since 1950 was not sensitive and remained around 1.6 for the last six years. Collectively, these multiple lines of evidence showed that the satellite-based maps are more consistent with the status of self-organized criticality than the reference maps are.

5. Discussion

(1) Fire mapping with Landsat multi-temporal image analysis using GEE

This study highlights the advantage of using image compositing approaches to identify the area burned, which does not require any prior knowledge about specific fire dates. This is especially important in remote locations where multiple fires are happening in different locations and times throughout the fire season. In addition to avoiding the issue of which day to choose images (Verbyla et al., 2008), this technique provides a mask to keep the area burned within the last ten years

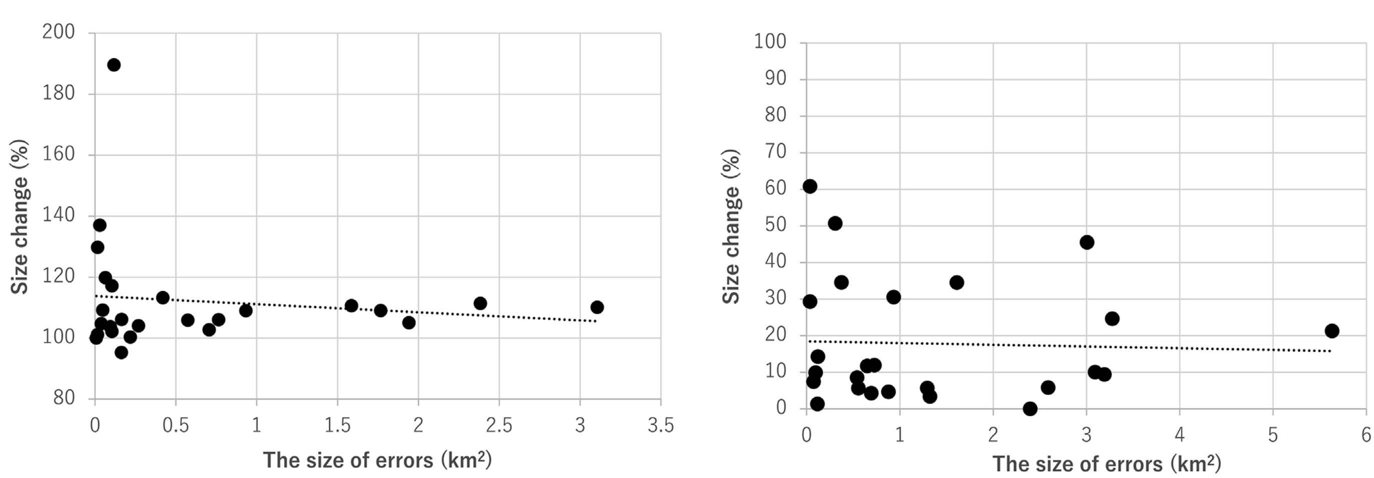

Fig. 9. Change of errors by noise filtering (left: commission error, right: omission error, more than 100% means increasing errors and less than 100% means decreasing errors relative to 100% which is set to the area of errors before the noise filtering was applied).

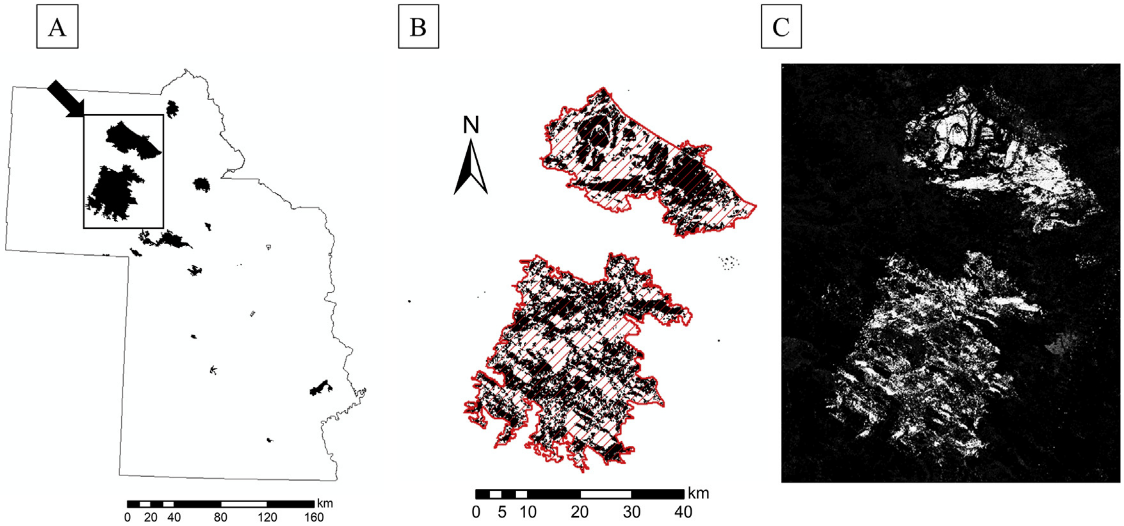

Fig. 10. Issues of producer's accuracy within the referenced fire map (producer's accuracy is 48.5% for this case. A: the location from 2004 data in our research site, B: the black area is a binary image to indicate the area burned with the shaded polygon from the referenced fire map, C: the original RdNBR image ranged from black to white to show low to high RdNBR value).

to avoid duplicating recently burned locations or to quantify patterns of recurring fire. Ten years represent a window wherein vegetation and fuel recovery generally precludes a new fire in the same location in this study area, but this window can be variable among different sites and species (Larsen, 1997). Moreover, this masking technique is useful to monitor ecological responses after fire because the mask can track post-fire trajectories of vegetation change within a given burned area.

An advantage of this study is the application of spectral indices such as NDVI and NBR (and RdNBR) to find the Best-Available-Pixel (White et al., 2017) for pre and post fire condition through the pixel-based image compositing (White et al., 2017). In this way, the first phase process in the two-phase algorithm (Bastarrika et al., 2011) can be simplified, because spectral indices are integrated to the pixel-based image compositing. In addition, we introduced and applied multi-step noise-filtering during post-processing to reduce confusion errors. In future studies, the Best-Available-Pixel can be improved by increasing images from more frequent satellite observations or integrating additional sensors such as Sentinel. The second phase of the two-phase algorithm (Bastarrika et al., 2011) uses an iterative region growing and is computationally expensive when scaled over a large region.

Manually drawn fire maps have been used to demonstrate SOC in studies over a large area like this study (Hantson et al., 2016; Moreno et al., 2011), but our study showed the finer detail fire boundary provide a better fit for the log-log linear relationship on Figs. 11 and 12. The significant difference between satellite image analysis and manually digitizing on Fig. 10 has also been shown in previous research (Cocke et al., 2005; Reilly et al., 2017). Problems with detecting fire boundaries using manually digitized aerial photos are well known (Andison, 2012; Andison and McCleary, 2014). Within a given polygon, there are unburned or spectrally unchanged patches left by variable burn severity (Fig. 10). When unburned islands were excluded, the user's accuracy was increased by 10% with the reference fire map only contains outlined fire perimeters. This confirmed that the unburned and low-severity areas influenced the accuracy. The omission and commission errors were also associated with the reference data quality, demonstrating the advantage of using more fire perimeters as reference data.

Table 2
The power-law relationship of results (gof is *goodness-of-fit* from KS statistics).

	α	xmin (km2)	p-value	gof
Reference data (from 1990)	1.73	29.46	0.003	0.1066
Satellite result (from 1990)	1.91	0.49	0.083	0.0193

Another key uncertainty is associated with phenological differences between conifer and deciduous forests. The spectral difference approach employed in this study has the capacity to detect not only the area burned by fire but also the phenological changes within deciduous stands. For example, the misclassified burned area which should not be burned in Fig. 9 included the seasonal change in deciduous trees. This

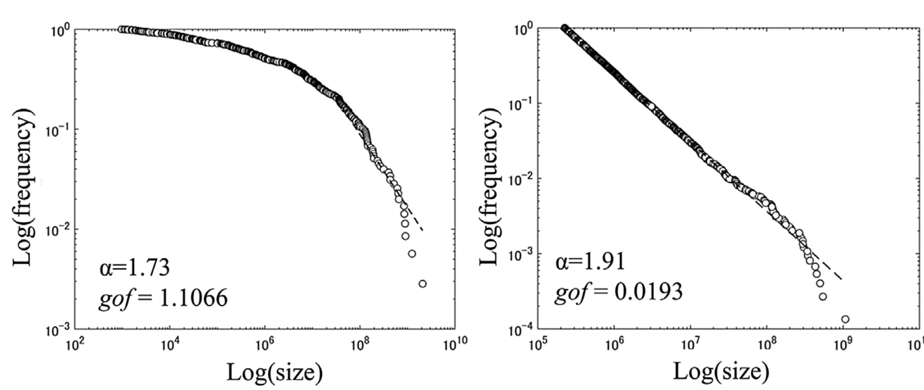

Fig. 11. Power law analysis of different data source from 1990 (left: the referenced fire map with *p* value < 0.05 of KS statistics, right: satellite result with *p* value > 0.05 of KS statistics).

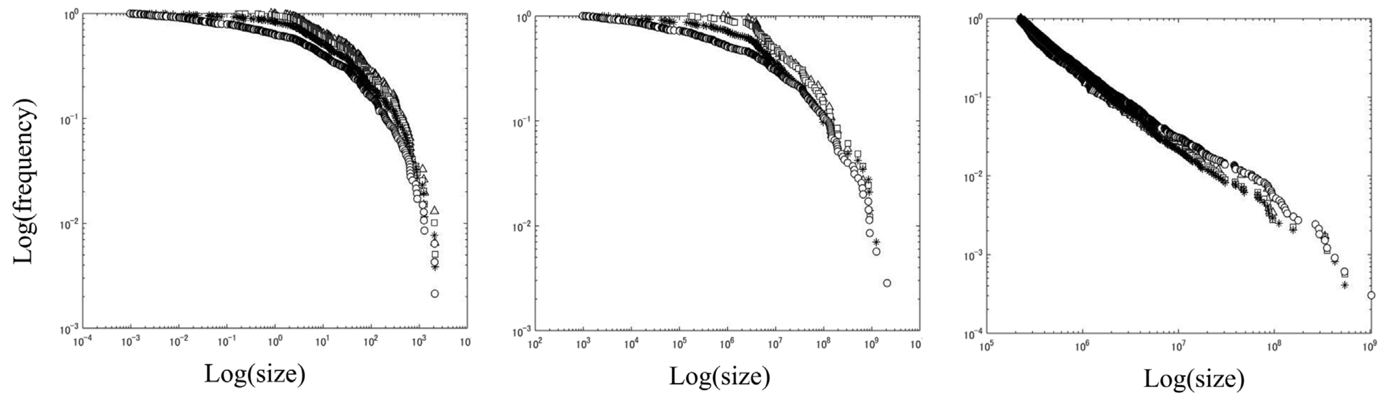

Fig. 12. Change of power-law relationship in different year intervals (left: reference data since 1950, center: reference data since 1990, right: RdNBR data since 1990, △ markers are years by 2000, □ markers are years by 2005, ∗ markers are years by 2010, ○ markers are years of all data by 2016.

issue exhibited a maximum error size of 1.19 km^2, which represents unavoidable errors associated with seasonal phenology. However, when we delineated seasonally deciduous forests with the Otsu threshold, the difference between pre- and post- NBR values over the burned area was larger than the difference due to seasonal change in the deciduous forest. Importantly, the same threshold technique can be applied to different ecosystem to account for local species composition.

One additional constraint of the technique used in this study is the range of input data from June 1st to September 30th, which limits the detection capability of spectral indices to snow-free time periods. When spectral indices are used as criteria to select images, the spectral sensitivity needs to be considered for the seasonal range (e.g. short-wave infrared red is sensitive to snow condition). Future application of this technique is in other regions could leverage thermal images to exclude snow from images while including data from a broader date range.

(2) General trends of fire with the concept of self-organized criticality

To date, forest fire events have been recognized as exhibiting SOC in simulation-based studies (Drossel and Schwabl, 1992; Hergarten, 2002) and with forest fire maps in natural stands of Yellowstone National Park (Malamud et al., 1998). In this study, Landsat time series indicated a power-law relationship, but the non-linear result from the reference fire map since 1990 did not follow the power-law (Fig. 11 and Table 2). Ricotta and co-authors (1999) found a similar result (i.e., non-linear, curved relationship) and they needed to divide the curve into several periods to fit the linear power-law relationships (Ricotta et al., 2001). Our study found that the curved shape comes from fire extent overestimation due to the outlined fire boundary (Fig. 10). Smaller fires are not influenced by this overestimation because the area tends to have more homogeneous severity and less complex perimeter patterns. However, larger fires are more susceptible to this overestimation because of mixed-severity mosaics within fire perimeters (Agee, 1993; Meddens et al., 2018).

In our study, the power-law relationship suggests that the Landsat data since 1990 provides a long enough record to assess general fire trends with the concept of SOC. However, questions remain in terms of how long the observation record needs to be to get reliable fire trends or how sensitive the slope is to the length of the time series and non-stationary behavior, such as recent increases in fire activity. From Fig. 12, the observation period from 1990 may not be long enough to stabilize the slope when compared with the slope created from 1950. This instability of the slope is reflected in the power-law distribution. As such, the sufficient time-series length depends on data quality. Our satellite results indicate that since 1990 the slope was around 2.0 and has not been changed by recent large fire events (Table 3).

In prior studies, the log-log slope was reported from 1.3 to 1.5 from Montana in the US, 1.1 to 2.0 in China, 2.2 from Californian in the US,

Table 3
The slope change of the power-law relationship in different intervals.

	Reference data since 1950	Reference data since 1990	RdNBR since 1990
by 2000	1.63 (50 years)	1.56 (10 years)	1.97 (10 years)
by 2005	1.66 (55 years)	1.51 (15 years)	2.00 (15 years)
by 2010	1.65 (60 years)	1.50 (20 years)	2.00 (20 years)
all data	1.67 (66 years)	1.73 (26 years)	1.91 (26 years)

and 1.0 to 1.2 from computer simulation result (Clauset et al., 2009; Malamud and Turcotte, 1999; Song et al., 2001). The slope difference was from the combustible materials (the amount of fuel), weather and climate (ecological zone), and fire suppression or control (fire frequency) (Malamud and Turcotte, 1999). Mandelbrot (1982) showed the fractal dimension is associated with α (the slope), and Song et al. (2001) compared the different fractal dimensions in different sites for SOC. In prior fire studies, the fractal index has been measured as the ratio between the perimeter and the area of the polygon (Turner et al., 2001) and our study shows how the slope difference between the reference map and the satellite result is influenced by the fractal dimensions of the fire boundary (Fig. 10).

The slope of SOC can be also related to the local fire behavior which is limited by abiotic or biotic condition such as topography and landscape physiography (Mansuy et al., 2014) and local ecozone (Parisien et al., 2006). For instance, fire behavior can be oriented along watershed (Barros et al., 2013, 2012). The local abiotic condition also determines general fire trends and patterns especially in boreal forest where climate is the limiting factor for forest fire. As such, landscape units such as watersheds or ecozones can be used to understand and interpret fire trends in the context of SOC.

Additional factors influencing the slope of SOC include input data resolution and human activity. The slope has been compared globally using 1 km resolution Moderate Resolution Spectroradiometer (MODIS) (Hantson et al., 2015b) and 30 m resolution Landsat imagery (Hantson et al., 2015a). Importantly, although the SOC concept itself is scale invariant and applicable to any scale of data, the slope can be variable from the input data from coarse to fine resolution (Hantson et al., 2015b). Because our study showed that the power-law slope was influenced by the perimeter or mosaic patterns, finer-resolution global coverage satellite such as Sentinel-2 (10 m resolution, ESA), RapidEye (5 m resolution, Planet Inc.), and Planetscope (3 m resolution, Planet Inc.) may confirm the optimum resolution to determine the slope of SOC. BA maps have already been created by Sentinel-2 over a large area of Africa (Roteta et al., 2019), and future studies could address SOC when the time series data archive is long enough.

Because the SOC slope was also influenced by human activity and socioeconomic dynamics (Hantson et al., 2015a, 2015b; Weiguo et al., 2006), it is important to assess potential shifting fire regimes in areas with and without substantial anthropogenic impacts. Our study site represents a good global reference site for boreal forests to understand how contemporary fire dynamics can be influenced by indirect anthropogenic impacts, including global warming.

Another key implication of this study is that if the site has been substantially disturbed by human activities, the site may not reach the critical state unless the human disturbance cycle is similar to the natural disturbance cycle. In the other words, this SOC concept can be a good indicator of sustainable landscapes adapted to fire disturbance within the historical range of variability. Testing criticality by power laws helps to understand general trends of contemporary fire regime, which could inform the sustainable use of prescribed fire and other management activities.

6. Conclusions

The rapid development of cloud-based satellite data analysis using GEE allows users to handle many images from satellite data archive without downloading the data. This study shows that Landsat time series composites can capture relatively fine-scale spatial patterning of fire perimeters, enabling the understanding of contemporary fire trends in a fire-prone area in boreal Canada, Wood Buffalo National Park. Our SOC assessment indicates that fire trends obtained from satellite data since 1990 followed a power-law relationship to produce the slope of 1.9, whereas the manually drawn reference map did not follow the power-law, potentially due to coarsely delineated fire perimeters. This technique reveals the fractal dimensionality of contemporary fire perimeters and establishes a baseline database for assessing future fire activity, which is likely to continue to increase in boreal forests. As such, this study elucidates fire trends directly from satellite data across a relatively large and remote boreal forest, which is very vulnerable to global warming.

Description of author's responsibilities

The corresponding author (Akira Kato) completed an original draft of this manuscript and conducted data analysis. All co-authors (David Thau, Andrew T. Hudak, Garret W. Meigs, and L.Monika Moskal) reviewed the manuscript and contributed to the writing process.

Funding

This research was supported by the Environment Research and Technology Development Fund of the Ministry of the Environment, Japan, grant number 2RF-1501.

Declaration of competing interest

The authors declare that they have no known competing financial interests or personal relationships that could have appeared to influence the work reported in this paper.

Acknowledgement

The authors would like to acknowledge Canadian Park Services for providing the fire maps. The authors especially thank Professor Akira Osawa (Kyoto University, Japan) and Nahoko Osawa-Kurachi for providing field data, Mizuki Taga (Olympus Co. Ltd., Japan), and Masuto Ebina (Hokkaido Research Organization, Japan) for their assistance for this study. This research is funded by Environment Research and Technological Development Fund, Ministry of the Environment, Japan, Project number: 2RF-1501. Additional support was provided by Oregon State University, USA. We also acknowledge two anonymous reviewers and editor who provided valuable feedback on the manuscript.

References

Agee, J.K., 1993. Fire Ecology of Pacific Northwest Forests. Island Press, Washington, D.C. https://doi.org/10.1071/WF9940195.

Albano, E.V., 1995. Spreading analysis and finite-size scaling study of the critical behavior of a forest fire model with immune trees. Phys. A Stat. Mech. its Appl. 216, 213–226. https://doi.org/10.1016/0378-4371(95)00015-Y.

Amiro, B.D., 2001. Fire, climate change, and carbon cycling in the boreal forest, agricultural and forest meteorology. https://doi.org/10.1016/S0168-1923(00)00218-5.

Andison, D.W., 2012. The influence of wildfire boundary delineation on our understanding of burning patterns in the Alberta foothills. Can. J. For. Res. 42, 1253–1263. https://doi.org/10.1139/x2012-074.

Andison, D.W., McCleary, K., 2014. Detecting regional differences in within-wildfire burn patterns in western boreal Canada. For. Chron. 90, 59–69. https://doi.org/10.5558/tfc2014011.

Bak, P., 1996. How Nature Works. Springer, New York.

Barbosa, P.M., Pereira, J.M.C., Gregoire, J.-M., Grégoire, J.M., 1998. Compositing Criteria for Burned Area Assessment Using Multitemporal Low. Remote Sens. Environ. 65, 38–49. https://doi.org/10.1016/S0034-4257(98)00016-9.

Barnosky, A.D., Hadly, E.A., Bascompte, J., Berlow, E.L., Brown, J.H., Fortelius, M., Getz, W.M., Harte, J., Hastings, A., Marquet, P.A., Martinez, N.D., Mooers, A., Roopnarine, P., 2012. Approaching a state shift in Earth ' s biosphere. Nature 486, 52–58. https://doi.org/10.1038/nature11018.

Barros, A.M.G., Moritz, M.A., Stephens, S.L., Florestais, C.D.E., 2013. Spatial characterization of wildfire orientation patterns in California. Forests 197–217. https://doi.org/10.3390/f4010197.

Barros, A.M.G., Pereira, J.M.C., Lund, U.J., 2012. Identifying geographical patterns of wildfire orientation : a watershed-based analysis. For. Ecol. Manage. 264, 98–107. https://doi.org/10.1016/j.foreco.2011.09.027.

Bastarrika, A., Chuvieco, E., Martín, M.P., 2011. Mapping burned areas from landsat TM/ ETM+ data with a two-phase algorithm: balancing omission and commission errors. Remote Sens. Environ. 115, 1003–1012. https://doi.org/10.1016/j.rse.2010.12.005.

Bowman, D.M.J.S., Balch, J., Artaxo, P., Bond, W.J., Cochrane, M.A., D'Antonio, C.M., Defries, R., Johnston, F.H., Keeley, J.E., Krawchuk, M.A., Kull, C.A., Mack, M., Moritz, M.A., Pyne, S., Roos, C.I., Scott, A.C., Sodhi, N.S., Swetnam, T.W., 2011. The human dimension of fire regimes on Earth. J. Biogeogr. 38, 2223–2236. https://doi.org/10.1111/j.1365-2699.2011.02595.x.

Campos-Ruiz, R., Parisien, M.A., Flannigan, M.D., 2018. Temporal patterns of wildfire activity in areas of contrasting human influence in the Canadian boreal forest. Forests 9. https://doi.org/10.3390/f9040159.

Chuvieco, E., Englefield, P., Trishchenko, A.P., Luo, Y., 2008. Generation of long time series of burn area maps of the boreal forest from NOAA – AVHRR composite data Generation of long time series of burn area maps of the boreal forest from NOAA – AVHRR composite data. Remote Sens. Environ. 112, 2381–2396. https://doi.org/10.1016/j.rse.2007.11.007.

Chuvieco, E., Mouillot, F., Werf, G.R. Van Der, San, J., Tanase, M., Koutsias, N., García, M., Yebra, M., Padilla, M., Gitas, I., Heil, A., Hawbaker, T.J., Giglio, L., 2019. Historical background and current developments for mapping burned area from satellite Earth observation. Remote Sens. Environ. 225, 45–64. https://doi.org/10.1016/j.rse.2019.02.013.

Clauset, A., Shalizi, C.R., Newman, M.E.J., 2009. Power-law distributions in empirical data. SIAM Rev. 51, 661–703. https://doi.org/10.1137/070710111.

Cocke, A.E., Fulé, P.Z., Crouse, J.E., 2005. Comparison of burn severity assessments using Differenced Normalized Burn Ratio and ground data. Int. J. Wildland Fire 14, 189–198. https://doi.org/10.1071/WF04010.

Cohen, W.B., Yang, Z., Kennedy, R., 2010. Detecting trends in forest disturbance and recovery using yearly Landsat time series: 2. TimeSync - tools for calibration and validation. Remote Sens. Environ. 114, 2911–2924. https://doi.org/10.1016/j.rse.2010.07.010.

Drossel, B., Schwabl, F., 1992. Self-organized critical forest-fire model. Phys. Rev. Lett. 69, 1629–1632.

Epting, J., Verbyla, D., Sorbel, B., 2005. Evaluation of remotely sensed indices for assessing burn severity in interior Alaska using Landsat TM and ETM+. Remote Sens. Environ. 96, 328–339. https://doi.org/10.1016/j.rse.2005.03.002.

Falk, D.A., Heyerdahl, E.K., Brown, P.M., Farris, C., Fulé, P.Z., Mckenzie, D., Swetnam, T.W., Taylor, A.H., Horne, M.L. Van, 2011. Multi-scale controls of historical forest-fire regimes : new insights from fire-scar networks. Front. Ecol. Environ. 9, 446–454. https://doi.org/10.1890/100052.

Flannigan, M., Stocks, B., Turetsky, M., Wotton, M., 2015. Impacts of climate change on fire activity and fire management in the circumboreal forest. Glob. Chnage Biol. 15, 549–560. https://doi.org/10.1111/j.1365-2486.2008.01660.x.

French, N.H.F., Kasischke, E.S., Hall, R.J., Murphy, K.A., Verbyla, D.L., Hoy, E.E., Allen, J.L., 2008. Using Landsat data to assess fire and burn severity in the North American boreal forest region : an overview and summary of results. Int. J. Wildland Fire 17, 443–462.

Gillett, N.P., Weaver, A.J., Zwiers, F.W., Flannigan, M.D., 2004. Detecting the effect of climate change on Canadian forest fires. Geophys. Res. Lett. 31. https://doi.org/10.1029/2004GL020876.

Goodwin, N.R., Collett, L.J., 2014. Development of an automated method for mapping fi re history captured in Landsat TM and ETM + time series across Queensland, Australia. Remote Sens. Environ. 148, 206–221. https://doi.org/10.1016/j.rse.2014.03.021.

Gorelick, N., Hancher, M., Dixon, M., Ilyushchenko, S., Thau, D., Moore, R., 2017. Google earth engine: planetary-scale geospatial analysis for everyone. Remote Sens. Environ. 202, 18–27. https://doi.org/10.1016/j.rse.2017.06.031.

Hansen, M.C., Potapov, P.V., Moore, R., Hancher, M., Turubanova, S. a, Tyukavina, a, Thau, D., Stehman, S.V., Goetz, S.J., Loveland, T.R., Kommareddy, a, Egorov, a, Chini, L., Justice, C.O., Townshend, J.R.G., 2013. High-resolution global maps of. Science 850, 2011–2014. https://doi.org/10.1126/science.1244693.

Hantson, S., Lasslop, G., Kloster, S., Chuvieco, E., 2015a. Anthropogenic effects on global

mean fire size. Int. J. Wildland Fire 24, 589–596.
Hantson, S., Padilla, M., Corti, D., Chuvieco, E., 2013. Strengths and weaknesses of MODIS hotspots to characterize global fi re occurrence. Remote Sens. Environ. 131, 152–159. https://doi.org/10.1016/j.rse.2012.12.004.
Hantson, S., Pueyo, S., Chuvieco, E., 2016. Global fire size distribution : from power law to log-normal. Int. J. Wildland Fire 25, 403–412.
Hantson, S., Pueyo, S., Chuvieco, E., 2015b. Global fire size distribution is driven by human impact and climate. Glob. Ecol. Biogeogr. 24, 77–86. https://doi.org/10.1111/geb.12246.
Hawbaker, T.J., Vanderhoof, M.K., Beal, Y.J., Takacs, J.D., Schmidt, G.L., Falgout, J.T., Williams, B., Fairaux, N.M., Caldwell, M.K., Picotte, J.J., Howard, S.M., Stitt, S., Dwyer, J.L., 2017. Mapping burned areas using dense time-series of Landsat data. Remote Sens. Environ. 198, 504–522. https://doi.org/10.1016/j.rse.2017.06.027.
Hergarten, S., 2002. Self-Organized Criticality in Earth Systems. Springer, Berlin Heidelberg.
Kasischke, E.S., Christensen, J.N.L., Stocks, B.J., 1995. Fire, global warming, and the carbon. Balance of Boreal Forests 5, 437–451.
Kasischke, E.S., Turetsky, M.R., 2006. Recent changes in the fire regime across the North American boreal region - spatial and temporal patterns of burning across Canada and Alaska. Geophys. Res. Lett. 33. https://doi.org/10.1029/2006GL025677.
Keane, R.E., Hessburg, P.F., Landres, P.B., Swanson, F.J., 2009. The use of historical range and variability (HRV) in landscape management. For. Ecol. Manage. 258, 1025–1037. https://doi.org/10.1016/j.foreco.2009.05.035.
Kennedy, R.E., Yang, Z., Cohen, W.B., 2010. Detecting trends in forest disturbance and recovery using yearly Landsat time series: 1. LandTrendr - temporal segmentation algorithms. Remote Sens. Environ. 114, 2897–2910. https://doi.org/10.1016/j.rse.2010.07.008.
Key, C.H., Benson, N.C., 2006. Landscape assessment (LA): sampling and analysis methods. FIREMON fire eff. Monit. Invent. Syst. (General tech. Rep. RMRS-GTR-164-CD) LA1–LA55. https://doi.org/10.1002/app.1994.070541203.
Kochtubajda, B., Flannigan, M.D., Gyakum, J.R., Stewart, R.E., Logan, K.A., Nguyen, T.V., 2006. Lightning and fires in the Northwest Territories and responses to future climate change. Arctic 59, 211–221. https://doi.org/10.2307/40512795.
Krawchuk, M.A., Haire, S.L., Coop, J., Parisien, M.A., Whitman, E., Chong, G., Miller, C., 2016. Topographic and fire weather controls of fire refugia in forested ecosystems of northwestern North America. Ecosphere 7, e01632. https://doi.org/10.1002/ecs2.1632.
Krawchuk, M.A., Moritz, M.A., Parisien, M.A., Dorn, J. Van, Hayhoe, K., 2009. Global pyrogeography: the current and future distribution of wildfire. PLoS One 4, e5102. https://doi.org/10.1371/journal.pone.0005102.
Larsen, A.C.P.S., Macdonald, G.M., Ecology, S., Jan, N., 2012. An 840-year record of fire and vegetation in a boreal white spruce forest an 840-YEAR record OF fire and vegetation IN A boreal white spruce forest. America (NY) 79, 106–118.
Larsen, C.P.S., 1997. Spatial and Temporal variations in boreal forest fire in frequency variations and temporal Spatial Alberta. J. Biogeogr. 24, 663–673.
Lentile, L.B., Smith, A.M.S., Hudak, A.T., Morgan, P., Bobbitt, M.J., Lewis, S.A., Robichaud, P.R., 2009. Remote sensing for prediction of 1-year post-fire ecosystem condition. Int. J. Wildland Fire 18, 594–608.
Lu, D., Mausel, P., Brondizio, E., Moran, E., 2004. Change detection techniques. Int. Jounal Remote Sens. 25, 2365–2407. https://doi.org/10.1080/0143116031000139863.
MacDonald, G.M., Larsen, C.P.S., Szeicz, J.M., Moser, K.A., 1991. The reconstruction of boreal forest fire history from lake sediments: a comparison of charcoal, pollen, sedimentological, and geochemical indices. Quat. Sci. Rev. 10, 53–71. https://doi.org/10.1016/0277-3791(91)90030-X.
Malamud, B.D., Morein, G., Turcotte, D.L., 1998. Forest fires: an example of self-organized critical behavior. Science 281 (80-), 1840–1842.
Malamud, B.D., Turcotte, D.L., 1999. Self-organized criticality applied to natural hazards. Nat. Hazards 20, 93–116. https://doi.org/10.1073/pnas.012582199.
Mandelbrot, B.B., 1982. The Fractal Geometry of Nature. Times Books, New York.
Mansuy, N., Boulanger, Y., Terrier, A., Gauthier, S., Robitaille, A., Bergeron, Y., 2014. Spatial attributes of fire regime in eastern Canada : influences of regional landscape physiography and climate. Landsc. Ecol. 29, 1157–1170. https://doi.org/10.1007/s10980-014-0049-4.
Meddens, A.J.H., Kolden, C.A., Lutz, J.A., Abatzoglou, J.T., Hudak, A.T., 2018a. Spatiotemporal Patterns of Unburned Areas within Fire Perimeters in the Northwestern United States from 1984 to 2014: Ecosphere, vol. 9https://doi.org/10.1002/ecs2.2029.
Meddens, A.J.H., Kolden, C.A., Lutz, J.A., Smith, A.M.S., Cansler, C.A., Abatzoglou, J.T., Meigs, G.W., Downing, W.M., Krawchuk, M.A., 2018b. Fire refugia: what are they, and why do they matter for global change? Bioscience 68, 944–954. https://doi.org/10.1093/biosci/biy103.
Miller, J.D., Thode, A.E., 2007. Quantifying burn severity in a heterogeneous landscape with a relative version of the delta Normalized Burn Ratio (dNBR). Remote Sens. Environ. 109, 66–80. https://doi.org/10.1016/j.rse.2006.12.006.
Moreno, M.V., Malamud, B.D., Chuvieco, E., 2011. Wildfire frequency-area statistics in Spain. Procedia Environ. Sci. 7, 182–187. https://doi.org/10.1016/j.proenv.2011.07.032.
Otsu, N., 1979. A threshold selection method from glay-level histograms. IEEE Trans. Syst. Man, Cybenetics 9, 62–66. https://doi.org/10.1109/TSMC.1979.4310076.
Parisien, M.A.M., Peters, V.S., Wang, Y., Little, J.M., Bosch, E.M., Stocks, B.J.B.J., 2006. Spatial patterns of forest fires in Canada , 1980 – 1999. Int. J. Wildland Fire 15, 361–374.
Parks, S.A., Holsinger, L.M., Voss, M.A., Loehman, R.A., Robinson, N.P., 2018. Mean composite fire severity metrics computed with google earth engine offer improved accuracy and expanded mapping potential. Remote Sens. 10, 1–15. https://doi.org/10.3390/rs10060879.
Perry, D.A., 1995. Self-organizing systems across scales. Trees (Berl.) 10, 241–244.
Reilly, M.J., Dunn, C.J., Meigs, G.W., Spies, T.A., Kennedy, R.E., Bailey, J.D., Briggs, K., 2017. Contemporary Patterns of Fire Extent and Severity in Forests of the Pacific Northwest, USA (1985-2010). Ecosphere, vol. 8https://doi.org/10.1002/ecs2.1695.
Ricotta, C., Arianoutsou, M., Díaz-Delgado, R., Duguy, B., Lloret, F., Maroudi, E., Mazzoleni, S., Manuel Moreno, J., Rambal, S., Vallejo, R., Vázquez, A., 2001. Self-organized criticality of wildfires ecologically revisited. Ecol. Model. 141, 307–311. https://doi.org/10.1016/S0304-3800(01)00272-1.
Ricotta, C., Avena, G., Marchetti, M., 1999. The flaming sandpile: self-organized criticality and wildfires. Ecol. Model. 119, 73–77. https://doi.org/10.1016/S0304-3800(99)00057-5.
Roteta, E., Bastarrika, A., Padilla, M., Storm, T., Chuvieco, E., 2019. Development of a Sentinel-2 burned area algorithm : generation of a small fi re database for sub-Saharan Africa. Remote Sens. Environ. 222, 1–17. https://doi.org/10.1016/j.rse.2018.12.011.
Roy, D.P., Boschetti, L., Trigg, S.N., 2006. Remote sensing of fire severity: assessing the performance of the normalized burn ratio. IEEE Geosci. Remote Sens. Lett. 3, 112–116. https://doi.org/10.2737/RMRS-GTR-164.
Schoennagel, T., Balch, J.K., Brenkert-Smith, H., Dennison, P.E., Harvey, B.J., Krawchuk, M.A., Mietkiewicz, N., Morgan, P., Moritz, M.A., Rasker, R., Turner, M.G., Whitlock, C., 2017. Adapt to more wildfire in western North American forests as climate changes. Proc. Natl. Acad. Sci. 114, 4582–4590. https://doi.org/10.1073/pnas.1617464114.
Shapiro, L., Stockman, G., 2001. Computer Vision. Prentice Hall, Upper Saddle River, NJ. https://doi.org/10.1525/jer.2008.3.1.toc.
Siegfried, C., Barbara, D., Franz, S., 1996. Forest fires and other examples of self-organized criticality. J. Phys. Condens. Matter 8, 6803.
Skinner, W.R., Flannigan, M.D., Stocks, B.J., Martell, D.L., Wotton, B.M., Todd, J.B., Mason, J.A., Logan, K.A., Bosch, E.M., 2002. A 500 hPa synoptic wildland fire climatology for large Canadian forest fires, 1959-1996. Theor. Appl. Climatol. 71, 157–169. https://doi.org/10.1007/s007040200002.
Song, W., Weicheng, F., Binghong, W., Jianjun, Z., 2001. Self-organized criticality of forest fire in China. Ecol. Model. 145, 61–68. https://doi.org/10.1016/S0304-3800(01)00383-0.
Soulard, C.E., Albano, C.M., Villarreal, M.L., Walker, J.J., 2016. Continuous 1985-2012 Landsat monitoring to assess fire effects on meadows in Yosemite National Park, California. Remote Sens. 8, 1–16. https://doi.org/10.3390/rs8050371.
Soverel, N.O., Coops, N.C., Perrakis, D.D.B., Daniels, L.D., Gergel, S.E., 2011. The transferability of a dNBR-derived model to predict burn severity across 10 wildland fires in western Canada. Int. J. Wildland Fire 20, 518–531. https://doi.org/10.1071/WF10081.
Soverel, N.O., Perrakis, D.D.B., Coops, N.C., 2010. Estimating burn severity from Landsat dNBR and RdNBR indices across western Canada. Remote Sens. Environ. 114, 1896–1909. https://doi.org/10.1016/j.rse.2010.03.013.
Stocks, B.J., Mason, J.A., Todd, J.B., Bosch, E.M., Wotton, B.M., Amiro, B.D., Flannigan, M.D., Hirsch, K.G., Logan, K.A., Martell, D.L., Skinner, W.R., 2002. Large forest fires in Canada, 1959–1997. J. Geophys. Res. 108, 8149. https://doi.org/10.1029/2001JD000484.
Sugihara, N.G., Van Wagtendonk, J.W., Shaffer, K.E., Fites-Kaufman, J., Thode, A.E., 2006. Fire in Calfornia's Ecosystems. University of Calfornia Press, Berkeley and Los Angeles, California.
Turner, M.C., Gardner, R.H., O`Neill, R.V., 2001. Landscape Ecology in Theory and Practice: Pattern and Process. Springer, New York.
Veraverbeke, S., Lhermitte, S., Verstraeten, W.W., Goossens, R., 2010a. The temporal dimension of differenced Normalized Burn Ratio (dNBR) fire/burn severity studies: the case of the large 2007 Peloponnese wildfires in Greece. Remote Sens. Environ. 114, 2548–2563. https://doi.org/10.1016/j.rse.2010.05.029.
Verbyla, D.L., Kasischke, E.S., Elizabeth, E.H., 2008. Seasonal and topographic effects on estimating fire severity from Landsat TM/ETM + data. Int. J. Wildland Fire 17, 527–534.
Verstraete, M.M., Pinty, B., 1996. Designing optimal spectral indexes for remote sensing applications - geoscience and remote sensing. IEEE Transactions on 34, 1254–1265.
Weiguo, S., Jian, W., Kohyu, S., Weicheng, F., 2006. Three types of power-law distribution of forest fires in Japan. Ecol. Model. 196, 527–532. https://doi.org/10.1016/j.ecolmodel.2006.02.033.
White, J.C., Wulder, M.A., Hermosilla, T., Coops, N.C., Hobart, G.W., 2017. A nationwide annual characterization of 25 years of forest disturbance and recovery for Canada using Landsat time series. Remote Sens. Environ. 194, 303–321. https://doi.org/10.1016/j.rse.2017.03.035.
White, J.C., Wulder, M.A., Hobart, G.W., Luther, J.E., Hermosilla, T., Griffiths, P., Coops, N.C., Hall, R.J., Hostert, P., Dyk, A., Guindon, L., 2014. Pixel-based image compositing for large-area dense time series applications and science. Can. J. Remote Sens. 40, 192–212. https://doi.org/10.1080/07038992.2014.945827.
Wilson, B.A., Ow, C.F.Y., Heathcott, M., Milne, D., Thomas, M., Ecology, S.G., Letters, B., Mar, N., Wilson, B.A., Ow, C.F.Y., Heathcott, M., Milne, D., Mccaffrey, T.M., Ghitter, G., Franklin, S.E., 2018. Landsat MSS Classification of Fire Fuel Types in Wood Buffalo National Park , Northern Canada McCaffrey , Geoff Ghitter and Steven E . Franklin Published By . Wiley Stable URL . http://www.jstor.org/stable/2997751 JSTOR is a not-for-profit service that he 4, 33–39.
Zhang, K., 2008. Identification of gaps in mangrove forests with airborne LIDAR. Remote Sens. Environ. 112, 2309–2325. https://doi.org/10.1016/j.rse.2007.10.003.
Zhu, Z., Woodcock, C.E., 2014. Continuous change detection and classification of land cover using all available Landsat data. Remote Sens. Environ. 144, 152–171. https://doi.org/10.1016/j.rse.2014.01.011.